Journal of Alloys and Compounds 509 (2011) 161–164

Contents lists available at ScienceDirect

Journal of Alloys and Compounds

journal homepage: www.elsevier.com/locate/jallcom

Thermoelectric and thermomechanical properties of the hot pressed polycrystalline $Bi_{0.5}Sb_{1.5}Te_3$ alloys

J.J. Shen, S.N. Zhang, S.H. Yang, Z.Z. Yin, T.J. Zhu, X.B. Zhao*

State Key Laboratory of Silicon Materials and Department of Materials Science and Engineering, Zhejiang University, Hangzhou 310027, China

ARTICLE INFO

Article history:
Received 10 June 2010
Received in revised form 30 August 2010
Accepted 1 September 2010
Available online 21 September 2010

Keywords:
$Bi_{0.5}Sb_{1.5}Te_3$ alloys
Thermoelectric properties
Thermomechanical properties

ABSTRACT

The polycrystalline pseudo-binary $Bi_{0.5}Sb_{1.5}Te_3$ alloys have been prepared by hot pressing. X-ray diffraction analysis indicated that there is no noticeable preferred orientation in all the samples. Thermoelectric properties were measured and a relatively high ZT value of ~0.9 was obtained at room temperature. Thermal mechanical properties were characterized by dilatometer and dynamic-mechanical thermal analyzer. The thermodynamic stability of these alloys could be kept from room temperature to 500 K. It is suggested that $Bi_{0.5}Sb_{1.5}Te_3$ alloys are suitable for the applications below 500 K.

1. Introduction

Thermoelectric (TE) devices have attracted many attentions due to their ability of quietly converting low quality heat from different sources into electricity [1,2]. The performance of thermoelectric materials can be represented by the dimensionless figure of merit $ZT = (\alpha^2\sigma/\kappa)T$, where α is the Seebeck coefficient, σ is the electrical conductivity, κ is the total thermal conductivity including the lattice contribution κ_l, bipolar contribution κ_b and the carrier contribution κ_e, and T is the absolute temperature [2,3]. Accordingly, a good TE material has to combine both high electrical power factor ($PF = \alpha^2\sigma$) and low thermal conductivity together [4]. Therefore, one crucial way to improve thermoelectric performance is to reduce the thermal conductivity without affecting the electric properties significantly.

Nowadays, most of the commercial thermoelectric devices operating near room temperature are built by bismuth telluride and its alloys. Although studied for more than 50 years, they are still the most important thermoelectric materials due to their excellent TE performance with the maximum ZT values of ~1 [1,5]. Traditionally, Bi_2Te_3-based alloys are prepared by unidirectional crystal-growth methods such as Bridgman and zone-melting techniques. The resultant crystals present good TE properties in the plane perpendicular to c-axis. However, there are also some side effects, such as their poor mechanical properties [4]. As for the further applications in devices, not only TE performance but also the mechanical properties should be considered. Therefore, powder metallurgy techniques combining with advanced sintering techniques have been considered to be effective ways to improve both the thermoelectric and mechanical properties [6–10]. For example, utilizing low-temperature hydrothermal method, ball milling and rapid solidification, combining hot pressing (HP), structural modulations (such as nanostructures) and related physical effects have been successfully introduced into bulk materials, and relatively high thermoelectric performances have been achieved [11–17]. Some mechanical properties study in Bi_2Te_3-based alloys have testified that polycrystalline bulk alloys prepared by powder metallurgy (sintered by hot pressing or spark plasma sinter) performed better bending strength than the unidirectionally grown ingots at room temperature [18,19]. On the other hand, the temperature dependence of thermal mechanical properties should be one important factor for the applications of TE materials owing to the thermal cycling working circumstance of TE devices. To our knowledge, there are limited reports on the temperature dependence of mechanical properties, which might provide helpful information to enhance the reliability of TE modules.

In the present work, polycrystalline pseudo-binary $Bi_{0.5}Sb_{1.5}Te_3$ alloys have been prepared by power metallurgy technique via different original ingots. The thermoelectric and thermal mechanical properties have been evaluated.

2. Experimental

Two different commercial p-type $Bi_{0.5}Sb_{1.5}Te_3$ ingots and one self-melting p-type $Bi_{0.5}Sb_{1.5}Te_3$ ingot were pulverized using the agate mortar in atmosphere environment for about 30 min. The sizes of obtained powders are roughly controlled using the 300 mesh standard sieve. Bulk disk-shaped pellets of Ø12.7 mm × 2 mm were sintered by hot pressing in the graphite dies under 80 MPa pressure at 673 K for

* Corresponding author. Tel.: +86 571 87951451; fax: +86 571 87951451.
E-mail address: zhaoxb@zju.edu.cn (X.B. Zhao).

0925-8388/$ – see front matter © 2010 Elsevier B.V. All rights reserved.
doi:10.1016/j.jallcom.2010.09.014

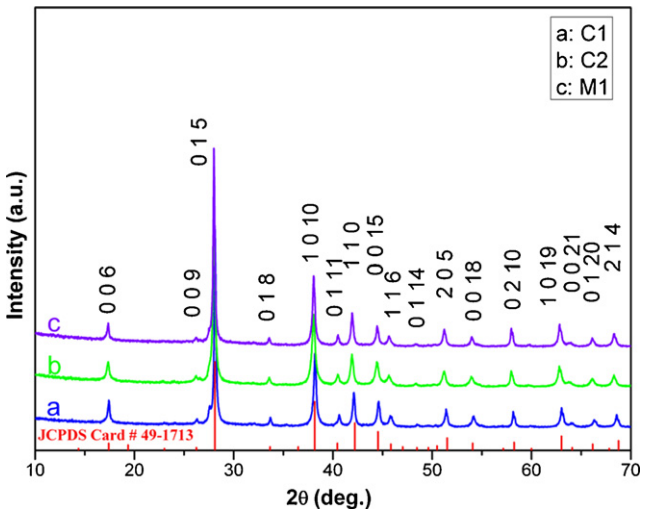

Fig. 1. XRD patterns of the $Bi_{0.5}Sb_{1.5}Te_3$ bulk samples prepared by powder metallurgy technique using different original ingots.

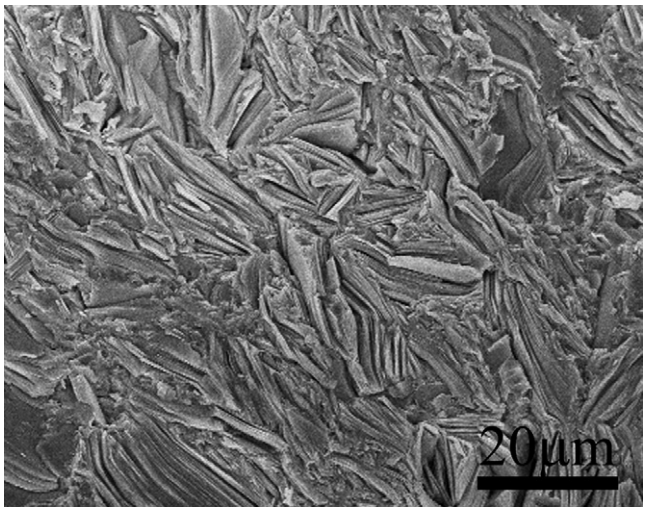

Fig. 2. SEM micrograph of the fracture surface of the C1 sample.

30 min in vacuum. The obtained samples were named as "C1, C2, and M1" according to the different initial ingots, which were two commercial ingots from two different companies and one self-melting ingot, respectively. The relative densities of the samples were >96% of the theoretical one characterized by Archimedes method.

The phase structures of the bulk samples were investigated by X-ray diffraction (XRD) with a Rigaku D/MAX-2550P diffractometer. The cross-section micromorphologies of the pellets were studied on the Hitachi S-4800 field emission scanning electron microscope (FESEM). The Seebeck coefficient α and electrical conductivity σ were simultaneously recorded using a DC four-probe method and differential voltage/temperature technique [20]. The thermal diffusivity D parallel to the hot pressing direction and specific heat C_p were determined on Netzsch® LFA 457 laser flash apparatus with a Pyroceram standard and Netzsch® Differential Scanning Calorimeters (DSC) 404C thermal analyzer, respectively [21]. The thermal conductivity κ was calculated as $\kappa = D\rho_D C_p$, where ρ_D is the density. The errors for electrical and thermal measurements are evaluated to be within 5% and 7%, respectively. The Netzsch® DIL 402 PC Dilatometer was used to investigate the thermal expansions of the samples, and the Netzsch® Dynamic-Mechanical Analyzer (DMA) 424 was used to characterize the temperature dependence compression and bending displacements. All the thermomechanical properties are measured parallel to the hot pressing direction. The thermogravimetric (TG) and DSC analysis were also carried out on the TA Instruments SDT Q600 thermogravimetric analyzer and Netzsch® DSC 404C, respectively, to survey the thermal stability of the samples.

3. Results and discussion

Fig. 1 shows the XRD patterns of the three pellets prepared by hot pressing. All the characteristic peaks of the bulk samples can be indexed into rhombohedral $Bi_{0.5}Sb_{1.5}Te_3$ phase with no impurities, indicating the single phase structure of these samples. Since

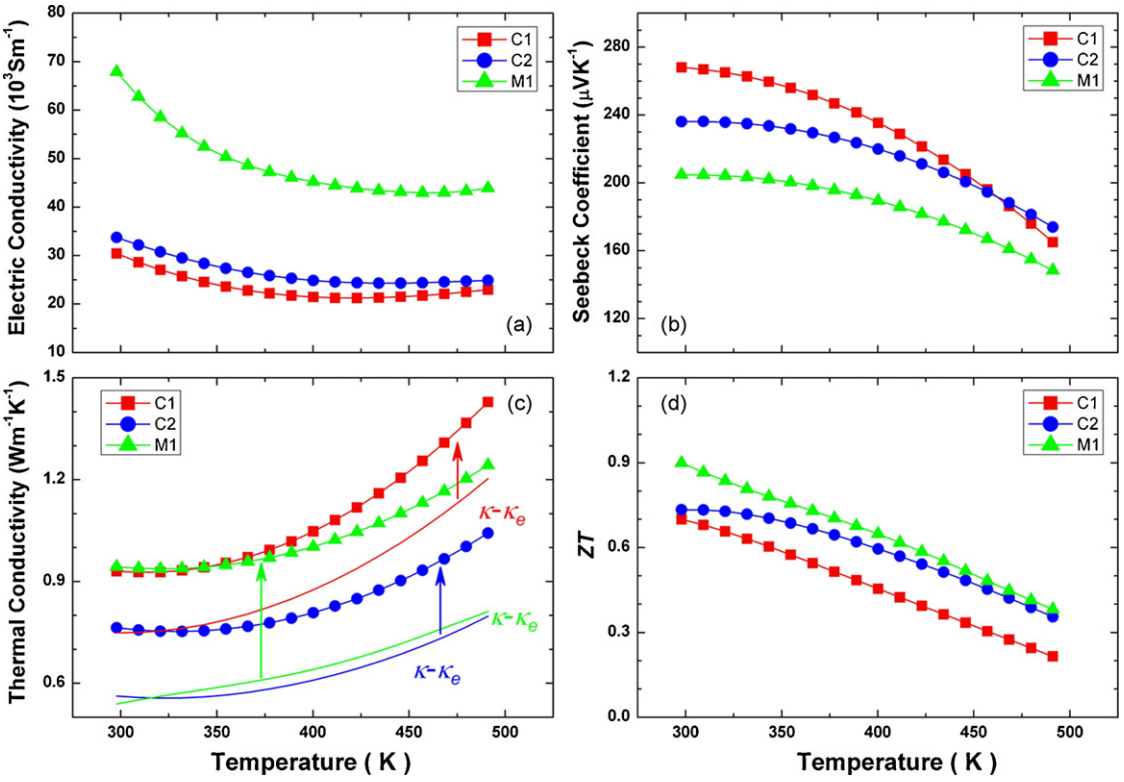

Fig. 3. Temperature dependences of thermoelectric properties of the $Bi_{0.5}Sb_{1.5}Te_3$ bulk samples: (a) the electrical conductivity, (b) the Seebeck coefficient, (c) the thermal conductivity, and (d) ZT value.

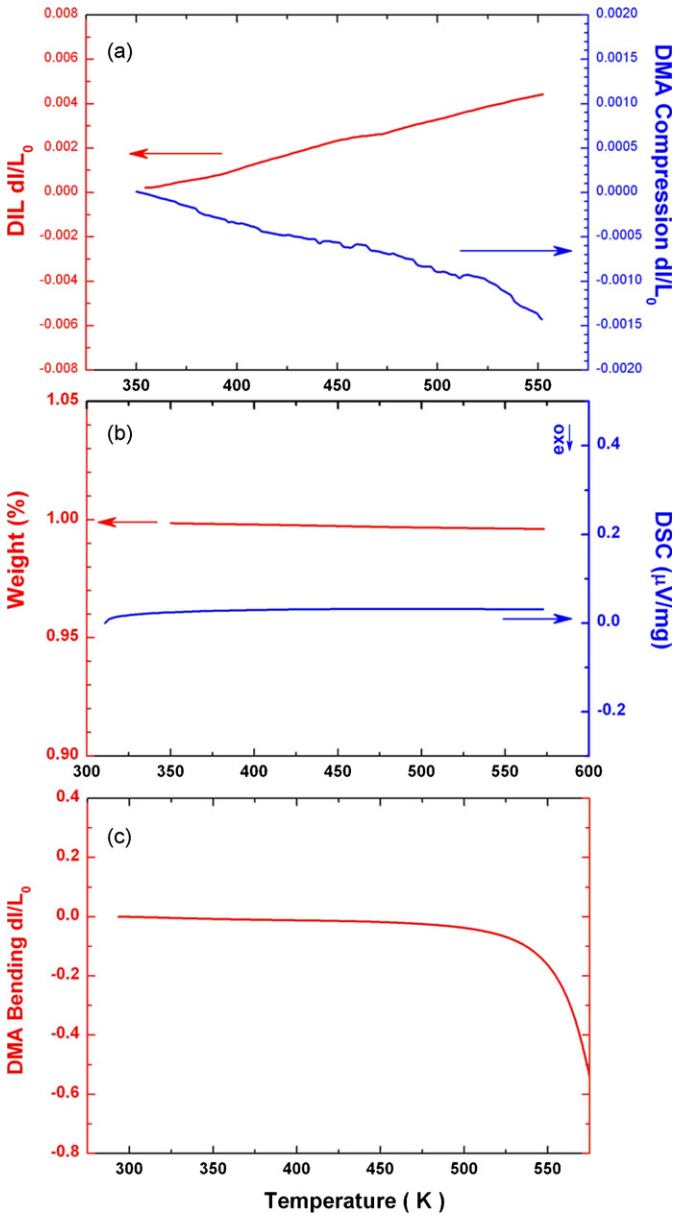

Fig. 4. Temperature dependences of thermal mechanical properties and thermal analysis of the $Bi_{0.5}Sb_{1.5}Te_3$ bulk sample M1: (a) the DIL thermal expansion and DMA compression, (b) the TG and DSC, and (c) the DMA bending.

the rhombohedral Bi_2Te_3 based alloys have a quasi-layered crystal structure, it is important to determine whether all these hot pressed samples are textured or not. The Orientation Factor *F*, which was used to quantitatively investigate the degree of preferred orientation of (0 0 *l*)-planes from the XRD results, is defined by the following formulae [22]:

$$F = \frac{P - P_0}{1 - P_0} \quad (1)$$

$$P_0 = \frac{I_0(0\,0\,l)}{\sum I_0(h\,k\,l)}, \qquad P = \frac{I(0\,0\,l)}{\sum I(h\,k\,l)} \quad (2)$$

where $I_0(h\,k\,l)$ and $I(h\,k\,l)$ are the peak integral intensities for randomly oriented sample and measured samples, respectively. P_0 and P are the ratios of the integrated intensities of all (0 0 *l*) planes to those of all ($h\,k\,l$) planes for randomly oriented and our samples, respectively. Because the grain sizes were within micrometer range and all the samples were prepared under the same condition, the values of *F* values were similar, which were 0.10, 0.08 and 0.07 for C1, C2 and M1 respectively. The results were slightly smaller than those of the previously reported hot-pressed and plasma activated sintered Bi_2Te_3 based alloys [23–25]. It is evidenced that all our samples are almost isotropic without noticeable texture [26].

Fig. 2 indicates the SEM image of cross-sectional surface of the C1 sample. The polyhedral sheet-like grains were randomly arranged with an average grain size in the vicinity of ~20 μm without preferred grain orientation. The other two samples, C2 and M1, exhibited the similar microstructures due to the same sintering method. These results are consistent with the XRD analysis in Fig. 1.

The temperature dependences of thermoelectric properties are plotted in Fig. 3. As shown in Fig. 3(a), the electrical conductivities of all these samples exhibit negative temperature dependence, suggesting the metal-like conduction behavior. The electric conductivities of M1 are $\sim 7 \times 10^4\ S\ m^{-1}$ at room temperature, higher than the other two samples ($\sim 3 \times 10^4\ S\ m^{-1}$ at room temperature). Generally speaking, there are mainly two factors can lead to the electrical conductivity differences, the carrier concentration and mobility. The carrier concentration is mainly related to the composition, while the mobility can be affected by the grain size, grain boundary density, and defects. In this work, considering that the preparation condition of all these three samples were the same, which means the grain size and grain boundary density could be comparable. Thus, the differences on electrical conductivities could be contributed to the different carrier concentration caused by the compositions.

All the samples exhibit the p-type semiconductor behavior over the measured temperature range, as shown in Fig. 3(b). The Seebeck coefficients of C1 and C2 samples achieve relatively higher values of ~270 μV/K and 240 μV/K at room temperature, respectively, while the maximum α value of M1 is only ~200 μV/K. Generally speaking, the Seebeck coefficient is inversely proportional to the carrier concentration. So the change of Seebeck coefficient is consistent with the change of carrier concentration. Based on the metal-like transport behavior, the Seebeck coefficients of all the three samples decrease with increasing temperature and reach a maximum value at about 300 K.

Fig. 3(c) shows the thermal conductivity as a function of temperature for the three samples. Note that all samples present extremely low thermal conductivities of <1 $W\ m^{-1}\ K^{-1}$. The sample C1 and M1 exhibit the similar thermal conductivities of 0.92 $W\ m^{-1}\ K^{-1}$, while that of the sample C2 is only 0.78 $W\ m^{-1}\ K^{-1}$. Considering the total thermal conductivity as the sum of three components, κ_e, κ_l and κ_b, the carrier thermal conductivity κ_e could be easily estimated by the Wiedemann–Franz relationship $\kappa_e = L_0\sigma T$ using the Lorenz number of $2.0 \times 10^{-8}\ V^2\ K^{-2}$, while the lattice and bipolar contribution could be presented as κ–κ_e [27]. Although the total thermal conductivities of C1 and M1 are almost the same at room temperature, the κ–κ_e value of M1 is remarkably lower than that of C1, which is only 0.55 $W\ m^{-1}\ K^{-1}$ and similar with the κ–κ_e value of C2. Furthermore, even after 'subtracting' the carrier component from the total thermal conductivities, the values of κ–κ_e still increase with temperature. Theoretically speaking, the lattice thermal conductivity should decrease with temperature, so the increasing trends should be attributed to the bipolar thermodiffusion effect [28]. Because the bismuth telluride based alloys are a series of narrow-gap semiconductors, the intrinsic excitation takes place at very low temperature with reasonably large contributions to the carrier concentrations, which also lead to the obvious increase in the thermal conductivity [29]. In fact, with the electrical conductivities increasing after 400 K, the slopes of κ and κ–κ_e became quite sharper.

Fig. 3(d) shows the dimensionless figure of merit, *ZT*, as a function of temperature for the three samples. The maximum *ZT* value measured at 300 K is about 0.9 for the sample M1, and those of

C1 and C2 are around 0.7. The *ZT* values in this study are comparable with that of the conventional commercial p-type material, but still lower than those of the nanostructure p-type Bi_2Te_3 based alloys [11–14]. Although the Seebeck coefficients and thermal conductivities were both well controlled, the low electrical conductivities still limited the final TE performance of the samples.

Mechanical properties are extremely important for the productions and applications of TE materials. Since all these three samples exhibited the similar TE performance and microstructures, one sample, M1, has been chosen as an example for mechanical property measurements and the results are shown in Fig. 4. The thermal expansion behavior as a function of temperature is shown in Fig. 4(a). The sample expanded slowly with increasing temperature. However, the thermal expansion result can only exhibit what will happen when the materials are heated without any structural constraint. While in the practical applications, all the materials will be made into legs and stuck to the substrates and there would be some compression stress applied on them during heating process. Therefore, the DMA compression test was taken to simulate the real situation and the data are also plotted in Fig. 4(a). It is obvious that the sample has been compressed when temperature increases. The decrement is only 0.2% after the measurement, which implies that there would be no significant change when the materials or devices are operating. In the meantime, the slopes of the two curves in Fig. 4(a) did not change within the entire temperature range, suggesting no phase transformation during the heating process. Moreover, the results of TG and DSC are also tested. As shown in Fig. 4(b), the two nearly horizontal lines suggested the alloys were technical thermodynamic stable. Fig. 4(c) shows the DMA bending test results which exhibit as the displacement–temperature curve. The sample displays little change from room temperature to 500 K while the curve drops sharply after 500 K. These results indicate that the $Bi_{0.5}Sb_{1.5}Te_3$ alloy would become soft and might be not suitable for application above 500 K.

4. Conclusions

In summary, polycrystalline $Bi_{0.5}Sb_{1.5}Te_3$ alloys have been prepared by powder metallurgy technique using different original ingots. The maximum dimensionless figure of merit *ZT* reaches about 0.9 at room temperature, comparable to that of unidirectionally grown commercial ingots. The thermal mechanical properties and thermal stabilities of a typical sample have also been investigated. The results indicated $Bi_{0.5}Sb_{1.5}Te_3$ alloys are appropriate for the practical application from room temperature up to 500 K.

Acknowledgments

We acknowledge the support of the Natural Science Foundation of China (50731006), the National “973” Program of China (2007CB607502), the National “863” Hi-tech Program of China (2007AA03Z234), the Zhejiang Provincial Natural Science Foundation (Z4090204) and the Scientific and Technological Program of Zhejiang Province (2009C34007).

References

[1] T.M. Tritt, Science 283 (1999) 804–805.
[2] F.J. DiSalvo, Science 285 (1999) 703–706.
[3] M.S. Dresselhaus, G. Chen, M.Y. Tang, R.G. Yang, H. Lee, D.Z. Wang, Z.F. Ren, J.P. Fleurial, P. Gogna, Adv. Mater. 19 (2007) 1043–1053.
[4] D.M. Rowe, CRC Handbook of Thermoelectrics, CRC Press, Boca Raton, 1995.
[5] D.Y. Chung, T. Hogan, P. Brazis, M. Rocci-Lane, C. Kannewurf, M. Bastea, C. Uher, M.G. Kanatzidis, Science 287 (2000) 1024–1027.
[6] C.D. Moon, S. Shin, D.H. Kim, T.S. Kim, J. Alloys Compd. 504S (2010) S504–S507.
[7] Y.L. Li, J. Jiang, G.J. Xu, W. Li, L.M. Zhou, Y. Li, P. Cui, J. Alloys Compd. 480 (2009) 954–957.
[8] L.D. Zhao, B.P. Zhang, W.S. Liu, H.L. Zhang, J.F. Li, J. Alloys Compd. 467 (2009) 91–97.
[9] X. Fan, J.Y. Yang, W. Zhu, S.Q. Bao, X.K. Duan, Q.Q. Zhang, J. Alloys Compd. 448 (2008) 308–312.
[10] C.H. Kuo, C.S. Hwang, M.S. Jeng, W.S. Su, Y.W. Chou, J.R. Ku, J. Alloys Compd. 496 (2010) 687–690.
[11] X.B. Zhao, X.H. Ji, Y.H. Zhang, T.J. Zhu, J.P. Tu, X.B. Zhang, Appl. Phys. Lett. 86 (2005) 062111.
[12] Y.Q. Cao, X.B. Zhao, T.J. Zhu, X.B. Zhang, J.P. Tu, Appl. Phys. Lett. 92 (2008) 143106.
[13] B. Poudel, Q. Hao, Y. Ma, Y.C. Lan, A. Minnich, B. Yu, X. Yan, D.Z. Wang, A. Muto, D. Vashaee, X.Y. Chen, J.M. Liu, M.S. Dresselhaus, G. Chen, Z. Ren, Science 320 (2008) 634–638.
[14] Y. Ma, Q. Hao, B. Poudel, Y.C. Lan, B. Yu, D.Z. Wang, G. Chen, Z.F. Ren, Nano Lett. 8 (2008) 2580–2584.
[15] S.N. Zhang, T.J. Zhu, S.H. Yang, C. Yu, X.B. Zhao, J. Alloys Compd. 499 (2010) 215–220.
[16] J. Jiang, T. Aizawa, A. Yamamoto, T. Ohta, J. Alloys Compd. 309 (2000) 225–228.
[17] J.Y. Yang, X.A. Fan, R.G. Chen, W. Zhu, S.Q. Bao, X.K. Duan, J. Alloys Compd. 416 (2006) 270–273.
[18] J. Jiang, L.D. Chen, S.Q. Bai, Q. Yao, Q. Wang, Scripta Mater. 52 (2005) 347–351.
[19] H.S. Shin, H.P. Ha, D.B. Hyun, J.D. Shim, D.H. Lee, J. Phys. Chem. Solids 58 (1997) 671–678.
[20] J.J. Shen, X.X. Liu, T.J. Zhu, X.B. Zhao, J. Mater. Sci. 44 (2009) 1889–1893.
[21] J.W. Vandersande, C. Wood, A. Zoltan, D. Witterberger, in: D.W. Yarborough (Ed.), Thermal Conductivity, Plenum Press, New York, 1988, pp. 445–452.
[22] O. Ben-Yehuda, R. Shuker, Y. Gelbstein, Z. Dashevsky, M.P. Dariel, J. Appl. Phys. 101 (2007) 113707.
[23] L.D. Zhao, B.P. Zhang, J.F. Li, H.L. Zhang, W.S. Liu, Solid State Sci. 10 (2008) 651–658.
[24] X.A. Fan, J.Y. Yang, W. Zhu, H.S. Yun, R.G. Chen, S.Q. Bao, X.K. Duan, J. Alloys Compd. 420 (2006) 256–259.
[25] X.A. Fan, J.Y. Yang, R.G. Chen, W. Zhu, S.Q. Bao, Mater. Sci. Eng. A 438 (2006) 190–193.
[26] J.J. Shen, T.J. Zhu, X.B. Zhao, S.N. Zhang, S.H. Yang, Z.Z. Yin, Energy Environ. Sci. (2010), doi:10.1039/c0ee00012d.
[27] J.L. Mi, X.B. Zhao, T.J. Zhu, J.P. Tu, Appl. Phys. Lett. 92 (2008) 029905.
[28] H. Frohlich, C. Kittel, Physica 20 (1954), 1086–1086.
[29] H.J. Goldsmid, Proc. Phys. Soc. Sect. B 69 (1956) 203–209.